Progress in Nuclear Energy 93 (2016) 287–296

Contents lists available at ScienceDirect

Progress in Nuclear Energy

journal homepage: www.elsevier.com/locate/pnucene

On the improvements in neutronics analysis of the unit cell for the pebble-bed fluoride-salt-cooled high-temperature reactor

Zhifeng Li [a], Liangzhi Cao [a, *], Hongchun Wu [a], Qingming He [a], Wei Shen [a, b]

[a] School of Nuclear Science and Technology, Xi'an Jiaotong University, Xi'an, Shaanxi, 710049, China
[b] Canadian Nuclear Safety Commission, Ottawa, Ontario, Canada

ARTICLE INFO

Article history:
Received 27 April 2016
Received in revised form
23 August 2016
Accepted 3 September 2016
Available online 10 September 2016

Keywords:
Explicit random model
Chord length sampling
Thermal-neutron scattering effect
Resonance elastic scattering effect
PB-FHR

ABSTRACT

The stochastic characteristics of the randomly distributed coated-fuel particles, the thermal-neutron scattering effect of the fluoride-salt and the resonance elastic scattering effect of heavy nuclides were neglected in early neutronics studies on the Pebble-Bed Fluoride-salt-cooled High-temperature Reactor (PB-FHR). In order to assess the impact of these effects on the neutronics calculation, the stochastic effect is analyzed by applying the explicit random modeling approach and Chord Length Sampling method, the thermal-neutron scattering effect of the fluoride-salt is quantified by evaluating and processing a new thermal-neutron scattering data library, and the resonance elastic scattering effect is covered by using the Doppler Broadening Rejection Correction (DBRC) method in this work. According to the critical calculations of the PB-FHR pebble unit cells with different TRISO Packing Factor (TPF), the different stochastic modeling methods lead to a difference of k_{inf} by tens of pcm, the thermal scattering effect of 2LiF-BeF_2 results in a decreasement of k_{inf} by 104–290 pcm and the resonance elastic scattering effect leads to a decreasement of k_{inf} by 107–437 pcm, respectively. In addition, the thermal-neutron scattering effect and resonance elastic scattering effect can be addible, the total impact of the thermal scattering effect of 2LiF-BeF_2 and the resonance elastic scattering effect of heavy nuclide leads to a decreasement of k_{inf} by 204–747 pcm.

1. Introduction

The Pebble-Bed Fluoride-salt-cooled High temperature Reactor (PB-FHR) is a novel design which adopts low-pressure liquid fluoride-salt and high-temperature randomly distributed Tristructural-isotropic (TRISO) coated-fuel particles. Recent studies of fluoride-salt-cooled high-temperature reactor conceptual designs cover the Pebble Bed Advanced High Temperature Reactor (PB-AHTR) at UCB (Fratoni, 2008), Sm-AHTR at ORNL (Greene et al., 2010), large central-station AHTR at ORNL (Holcomb et al., 2011; Varma et al., 2012), the Pebble-Bed FHR at UCB (Krumwiede et al., 2013; Scarlat and Peterson, 2013), and the experimental pebble-bed fluoride-salt-cooled high-temperature reactor at Shanghai Institute of Applied Physics which will be constructed as an initial step to test and verify the technical feasibility of a large-scale reactor in the next years (SINAP, 2012; Xiao et al., 2014; Liu et al., 2016). However, some significant neutronics effects are ignored in early neutronics analysis of the PB-FHR. In addition, the distinctive characteristics of the PB-FHR are as follows:

The first characteristic of the PB-FHR is that the pebble-bed reactor core consists of randomly distributed fuel pebbles which are made of randomly distributed TRISO coated-fuel particles. This special structure is the so-called 'double-level random distribution'. However, in the preliminary neutronics analysis of the fluoride-salt-cooled high-temperature reactor (Qin et al., 2016), only regular lattice modeling method is applied. Recently some random modeling methods have been developed, for example, the explicit random modeling method is shown to be the most precise one among the Random Lattice Method, Chord Length Sampling (CLS) method and explicit random modeling method (Liu et al., 2015a). The explicit random modeling method has been implemented in the Monte-Carlo codes such as MONK (Smith et al., 2001), RMC (She et al., 2015; Liu et al., 2015b) and Serpent (Leppänen, 2012). In this work, the coordinates of the TRISO coated-fuel particles were read from a separate file generated by the in-house packing code PACK, then the coordinate file is used by Serpent to perform the Monte-Carlo simulation of PB-FHR pebble unit cell. Because the explicit

* Corresponding author.
E-mail address: caolz@mail.xjtu.edu.cn (L. Cao).

http://dx.doi.org/10.1016/j.pnucene.2016.09.004
0149-1970/

random model costs huge memory and needs reading the positions of the particles from a separate file, the CLS method as an alternative and less expensive method has been widely studied (Murata et al., 1996, 1997; Mori et al., 2000; Reinert, 2010), but the challenge of the CLS method is the boundary effect (Murata et al., 1996) which would influence the accuracy. Three kinds of correction technique have been proposed to improve the accuracy of the CLS method (Murata et al., 1996; Ji and Martin, 2008; Griesheimer, 2010), the latest nonlinear relationship correction technique (Griesheimer, 2010) is adopted when the TPF is high in this work. Since the explicit random model and CLS method have their advantages and disadvantages, the Monte-Carlo simulation results of the two methods are compared to analyze the stochastic effect of the PB-FHR and to decide which random method is adopted to obtain accurate Monte-Carlo transport calculation results for all the PB-FHR pebble unit cells in the following sections in this paper.

The second characteristic of the PB-FHR is that the coolant of the core is high-temperature fluoride-salt (2LiF-BeF_2). It is found that the moderating properties of 2LiF-BeF_2 are not negligible and the impact of the thermal-neutron scattering effect of 2LiF-BeF_2 on the neutronics calculation of MSRE is significant (Mei et al., 2013). However, the impact of the thermal-neutron scattering effect of 2LiF-BeF_2 on the neutronics calculation of PB-FHR has not been studied (Qin et al., 2016). The thermal-neutron scattering effect of the 2LiF-BeF_2 is quantified by re-evaluating and processing a new thermal-neutron scattering data library. In addition, the fuel of the PB-FHR core works at high temperatures. Recent studies show that the energy-dependent elastic scattering kernel of ^{238}U would considerably improve the precision of critical calculations for high-temperature reactors such as HTR and HTTR (Becker et al., 2009a). However, the impact of the resonance elastic scattering effect on the neutronics of PB-FHR has not been studied in early studies (Qin et al., 2016). In this study, the resonance elastic scattering effect of the ^{238}U is calculated by the Doppler Broadening Rejection Correction (DBRC) method.

The remainder of the paper is organized in the following manner: the methods of modeling the randomly distributed TRISO coated-fuel particles to quantify the stochastic effect are described in Section 2. Section 3 introduces the methods of re-evaluating and processing thermal-neutron scattering data libraries of the 2LiF-BeF_2. The ACE format continue-energy and WIMS format multi-group thermal-neutron scattering cross-section libraries are used by the Monte-Carlo code Serpent and deterministic code SUGAR to quantify the thermal-neutron scattering effect. Section 4 describes the DBRC method to quantify the resonance elastic scattering effect. Section 5 discuss the total impact of the thermal-neutron scattering effect and resonance elastic scattering effect. Finally conclusions and future work plans are given in Section 6.

2. Stochastic modeling methods

The PB-FHR adopts fuel pebbles with a 0.5 cm thickness graphite shell outside and 2.5 cm thickness graphite matrix inside which contains a large number of TRISO coated-fuel particles. The TRISO packing factor (TPF) is defined as the volume fraction of the TRISO coated-fuel particles in the matrix. The TPF of the PB-FHR fuel pebble in this paper varies from 5.02% to 30% which covers most of the existing PB-FHR designs. The TRISO coated-fuel particle, from inner to outer, consists of a UO_2 fuel kernel, porous carbon buffer layer, dense inner pyrolytic carbon layer, chemically vapor deposited silicon carbide layer, and dense outer pyrolytic carbon layer. A binary molten salt system of the 2LiF-BeF_2 (0.005% ^6Li) is used as the primary coolant. The volumetric filling fraction of pebbles in core is set to be 60.46%. The calculated atomic densities of the pebble unit cell (IAEA, 2003) are summarized in Table 1.

In order to quantify the stochastic effect of the PB-FHR pebble unit cell, the following two models are compared.

The first model is the explicit random modeling method, as shown in Fig. 1. Before performing the Monte-Carlo calculations, the random coordinate sampling for TRISO coated-fuel particles is calculated by the in-house packing code PACK. The calculation procedure is as follows: 1) uniformly sample a TRISO coated-fuel particle within the fuel zone of the pebble; 2) compare with all the other existing TRISO coated-fuel particles in the fuel zone to check if the newly sampled TRISO coated-fuel particles overlaps with any one of them; 3) the new particle will be accepted if there is no overlap, otherwise reject and resample. These steps continue until the desired TRISO packing factor is reached. The coordinates of the randomly distributed TRISO coated-fuel particles are then used as the input for subsequent Monte-Carlo calculations. The explicit random modeling method of Serpent treats the distributions of TRISO coated-fuel particles explicitly.

In order to obtain the actual k_{inf} of the PB-FHR pebble unit cell, 10 types of randomly distributed TRISO coated-fuel particles for one pebble unit cell are simulated. The coordinates of the randomly distributed TRISO coated-fuel particles of each type are randomly generated by the packing code PACK. The average value of the 10 types is used as the practical k_{inf}. The criticality calculation is performed by Serpent. Each Monte-Carlo calculation uses 100,000 neutrons per cycle, 10,500 active cycles and 500 inactive cycles. The standard deviation of k_{inf} is 0.00004. The results of these configurations are summarized in Table 2. It is found that the uncertainty $\sigma(\overline{k}_{\inf})$ caused by different types of random distribution is quite small.

The second random model called CLS method which is also implemented in the Monte Carlo code Serpent. A flag is set for the stochastic medium region, the CLS method is used when a neutron enters the flagged region. When a neutron enters a TRISO fuel particle, regular Monte Carlo procedures are applied. A chord length PDF (Liang et al., 2012) given by Eq. (1) is applied in the CLS to sample the distance to a TRISO fuel particle: 1) when a neutron enters the stochastic fuel zone; or 2) after a neutron flies off a TRISO fuel particle; or 3) after a neutron scatters in the graphite matrix.

$$f(l) = \frac{3}{4 \bullet r} \bullet \frac{TPF}{1 - TPF} \bullet e^{-l \bullet \frac{3}{4 \bullet r} \bullet \frac{TPF}{1 - TPF}} \tag{1}$$

where TRISO Packing Factor (TPF) is the TRISO fuel particle volume packing fraction in the pebble unit cell, r is the radius of the TRISO fuel particle.

The change of the CLS method is the accuracy related to the boundary effect (Murata et al., 1996), which is unavoidable when the CLS method is used in a finite stochastic media system (Liang and Ji, 2011). The boundary effect results from not allowing the overlap of the sampled fuel kernel with the system boundary. Re-sampling is performed in the CLS if an overlap happens (Murata et al., 1996; Ji and Martin, 2008), that would reduce TRISO Packing Factor (TPF) and finally lead to bring down the accuracy of the CLS method. Three kinds of correction technique has been proposed to improve the accuracy of the CLS method (Murata et al., 1996; Ji and Martin, 2008; Griesheimer, 2010), the latest nonlinear relationship correction technique (Griesheimer, 2010; Liang et al., 2012) is adopted when the TPF is high in this work. The corrected TPF and true TPF has a nonlinear relationship given by Eq. (2) which was derived based on modified Poisson approximation.

$$TPF' = 1 - \frac{R}{r} + \sqrt{\left(\frac{R}{r} - 1\right)^2 + 2\frac{R}{r} \bullet TPF} \tag{2}$$

where TPF' is the corrected TRISO packing factor and TPF is the true

Table 1
Geometry and composition of PB-FHR pebble unit cell.

Fuel pebble cell	Radius (cm)	Isotope and atom density (atom/barn-cm)
Fuel kernel	0.0250	^{235}U: 3.9500E-3; ^{238}U: 1.9286E-2; ^{16}O: 4.6472E-2; ^{10}B: 1.8495E-8; ^{11}B: 7.4445E-8
Carbon buffer layer	0.0340	C: 5.51524E-2
Inner pyrolytic carbon layer	0.0380	C: 9.52621E-2
Silicon carbide layer	0.0415	C: 4.77240E-2; ^{28}Si: 4.40125E-2; ^{29}Si: 2.23587E-3; ^{30}Si: 1.47563E-3.
Outer pyrolytic carbon layer	0.0455	C: 9.52621E-2
Graphite matrix	2.5000	C: 8.6738E-2; ^{10}B: 2.2439E-8; ^{11}B: 9.0321E-08
Pebble shell	3.0000	C: 8.6738E-2; ^{10}B: 2.2439E-8; ^{11}B: 9.0321E-08
Fluoride salt coolant		^{6}Li: 1.19185E-6; ^{7}Li: 2.38358E-2; ^{9}Be: 1.19185E-2; ^{19}F: 4.76740E-2

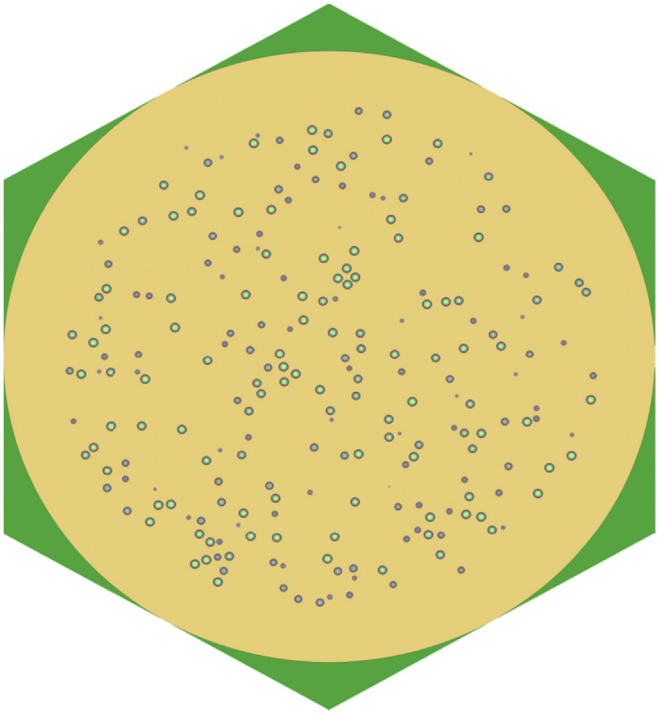

Fig. 1. PB-FHR pebble unit cell with randomly distributed TRISO coated-fuel particles (inner to outer is the fuel zone, pebble shell and fluoride-salt coolant).

TRISO packing factor, r is the radius of the TRISO fuel particle, R is the radius of the fuel zone of the pebble unit cell.

The k_{inf} of the explicit random modeling method and the CLS method of the PB-FHR pebble unit cells with different TPF are listed in Table 3. The TPF of a PB-FHR pebble ranges from 5.0% to 30%. It is found that the difference between the two modeling methods is not significant when TPF is low. However, when the TPF is 30%, the difference between the two modeling methods is not acceptable. Therefore the original CLS model implemented in Serpent seems to work best for low packing fractions. After using the correction technique, the difference between two random methods decrease significantly but still not negligible. Considering that the results of the explicit random method are stable and exact, only the explicit random modeling is adopted to obtain accurate Monte-Carlo transport calculation results for all the PB-FHR pebble unit cells in the following sections in this work.

Table 3
k_{inf} of the Explicit random method and CLS method for different TPF and temperature.

TPF/Pebble	5.02%	7.00%	10.0%	15.0%	30.0%	
Temperature (coolant: 900 K, other material: 1000 K)						
Explicit Random	1.48245	1.48827	1.46136	1.39876	1.25290	
Implicit Random	1.48151	1.48698	1.46056	1.39937	1.25801	1.25489[a]
Difference (pcm)	−63	−87	−55	44	408	159[a]
Temperature (coolant: 300 K, other material: 1000 K)						
Explicit Random	1.48251	1.48937	1.46288	1.40067	1.25404	
Implicit Random	1.48173	1.48800	1.46240	1.40146	1.25979	1.25637[a]
Difference (pcm)	−53	−92	−33	56	459	186[a]
Temperature (coolant: 900 K, other material: 1200 K)						
Explicit Random	1.47224	1.47617	1.44770	1.38287	1.23567	
Implicit Random	1.47135	1.47521	1.44682	1.38359	1.24070	1.23753[a]
Difference (pcm)	−60	−65	−61	52	407	151[a]

[a] Corrected by Eq. (2).

3. Thermal-neutron scattering effect of 2LiF-BeF_2

Lacking of the Thermal-neutron Scattering data Library (TSL) for 2LiF-BeF_2 results in the ignorance of thermal-neutron scattering effect of the 2LiF-BeF_2 in previous studies on PB-FHR (Qin et al., 2016). Only the thermal-neutron scattering effect of the graphite is considered in these studies. Besides, the TSL of 2LiF-BeF_2 is not available in the existing evaluated thermal-neutron scattering sub-libraries, therefore it's necessary to evaluate and process a new thermal-neutron scattering data library for 2LiF-BeF_2. According

Table 2
The k_{inf} of 10 types explicit random modeling for the PB-FHR pebble unit cell with TPF = 5.02% ($\overline{k}_{\inf} = \frac{1}{N}\sum_{i=1,N} k^i_{\inf}$, $\sigma(\overline{k}_{\inf}) = \sqrt{\frac{\sum_{i=1,N}(k^i_{\inf}-\overline{k}_{\inf})^2}{N-1}}$.

Explicit random types	k_{inf}	$\overline{k}_{\inf}$	$\sigma(\overline{k}_{\inf})$
1	1.48249		
2	1.48239		
3	1.48257		
4	1.48231		
5	1.48248	1.48245	0.00008
6	1.48246		
7	1.48245		
8	1.48235		
9	1.48245		
10	1.48256		

the theory of the thermal-neutron scattering, the thermal-neutron scattering cross section can be written as:

$$\sigma(E\to E',\mu)=\frac{\sigma_b}{2k_BT}\sqrt{\frac{E\prime}{E}}S(\alpha,\beta) \tag{3}$$

$$\alpha=\frac{E'+E-2\mu\sqrt{EE\prime}}{Ak_BT} \tag{4}$$

$$\beta=\frac{E'-E}{k_BT} \tag{5}$$

where E' is the scattered neutron energy, E is the incident neutron energy, α and β are the momentum transfer and the energy transfer respectively, σ_b is the characteristic scattering cross section for material, μ is the cosine of scattering angle, A is the mass ratio of the scatter nucleus to neutron, k_BT is the thermal energy in eV.

When the temperature of 2LiF-BeF_2 is below 774 K, using the Gaussian Approximation, the solid-type scattering function is written as:

$$S_s(\alpha,\beta)=\frac{1}{2\pi}\int_{-\infty}^{\infty}e^{i\beta t}e^{-\gamma(t)}\mathrm{d}t \tag{6}$$

$$\gamma(t)=\alpha\int_{-\infty}^{\infty}P_s(\beta)\left[1-e^{-i\beta t}\right]\times e^{-\beta/2}\mathrm{d}\beta \tag{7}$$

$$P_s(\beta)=\frac{\rho_s(\beta)}{2\beta\sinh(\beta/2)} \tag{8}$$

where $S_s(\alpha,\beta)$ is the solid-type scattering function, $\gamma(t)$ is the Gaussian function for solid-type frequency spectra, $\rho_s(\beta)$ is the frequency spectrum of excitations in the system and it is calculated by the CASTEP (Refson, 2004) as shown in Fig. 6. In view of the exchange-correlation of electrons, the Generalized Gradient Approximation method was applied. The phonon frequency corresponds to fundamental mode of vibration within 2LiF-BeF_2, as shown in Fig. 2.

The function $P_s(\beta)$ given by Eq. (8) is used directly in LEAPR module of NJOY code. Utilizing the phonon expansion, the scattering function defined by Eq. (6) can be written as:

$$S_s(\alpha,\beta)=e^{-\alpha\lambda_s}\sum_{n=0}^{\infty}\frac{1}{n!}\alpha^n \times\frac{1}{2\pi}\int_{-\infty}^{\infty}e^{i\beta t}\left[\int_{-\infty}^{\infty}P_s(\beta\prime)e^{-\beta\prime/2}e^{-i\beta\prime t}\mathrm{d}\beta\prime\right]^n\mathrm{d}t \tag{9}$$

For large values of α, the expansion of Eq. (9) requires extensive number of terms. Using the simple Short-Collision-Time (SCT) approximation from ENDF, the solid-type scattering law becomes:

$$S_s(\alpha,\beta)=\frac{1}{\sqrt{4\pi\omega_s\alpha\overline{T}_s/T}}\exp\left[-\frac{(\omega_s\alpha-\beta)^2}{\omega_s\alpha\overline{T}_s/T}\right] \tag{10}$$

whereω_s is the weight for the solid-type spectrum and the effective temperature $\overline{T}_s$ can be written as:

$$\overline{T}_s=\frac{T}{2\omega_s}\int_{-\infty}^{\infty}\beta^2P_s(\beta)e^{-\beta}d\beta \tag{11}$$

Because the LiF and BeF_2 are solids consisting of coherent scatterers, the zero-phonon term leads to interference scattering from atoms at various planes in lattices that making up the crystal. The coherent elastic scattering becomes:

$$\sigma_{coh}(E,\mu)=\frac{\sigma_c}{E}\sum_{E_i<E}f_ie^{-4WE_i}\delta(\mu-\mu_i) \tag{12}$$

where

$$\mu_i=1-E_i/E \tag{13}$$

and the integrated cross section can be written as:

$$\sigma_{coh}=\frac{\sigma_c}{E}\sum_{E_i<E}f_ie^{-4WE_i} \tag{14}$$

where W is the effective Debye-Waller coefficient, f_i are crystallographic structure factors, σ_c is the effective bound coherent scattering cross section and E_i are the Bragg Edges. Finally, the inelastic scattering cross section and coherent elastic scattering cross sections of BeF_2 and LiF at 350 K are shown in Figs. 3 and 4.

We can find that the thermal-neutron inelastic cross section curve is smooth (see the left of Figs. 3 and 4), however, the thermal-neutron coherent elastic cross section is zero below the first Bragg edge, then the coherent elastic cross section jumps sharply to a

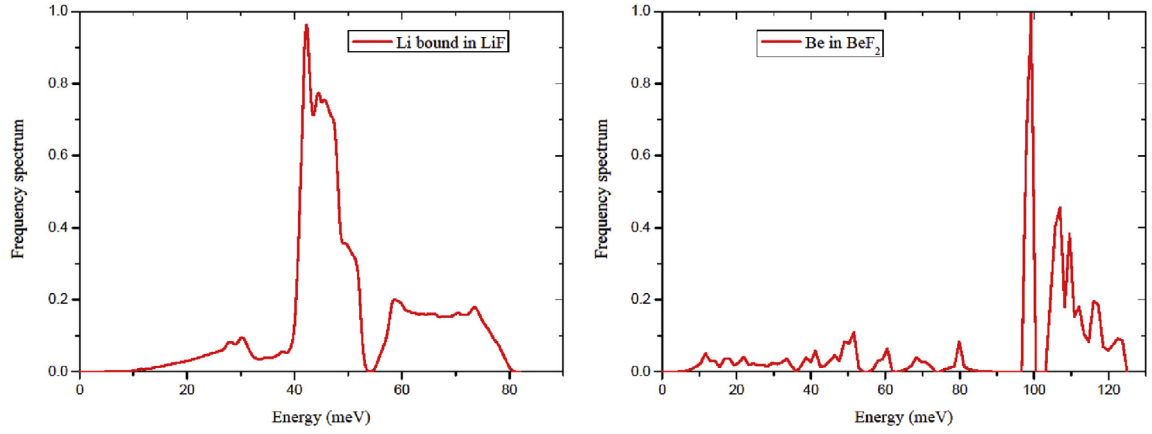

Fig. 2. Phonon frequency spectrum of Li bound in LiF and Be bound in BeF_2.

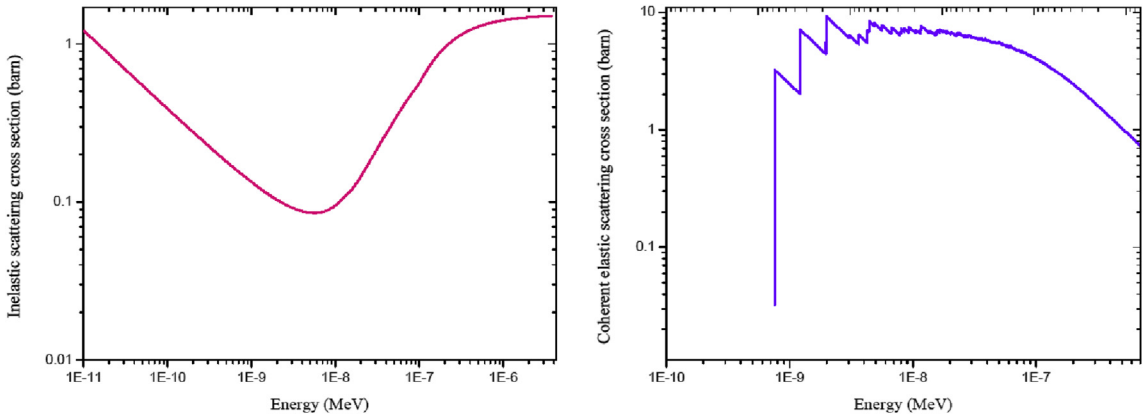

Fig. 3. Inelastic scattering cross section and coherent elastic scattering cross section of BeF_2 at 350 K.

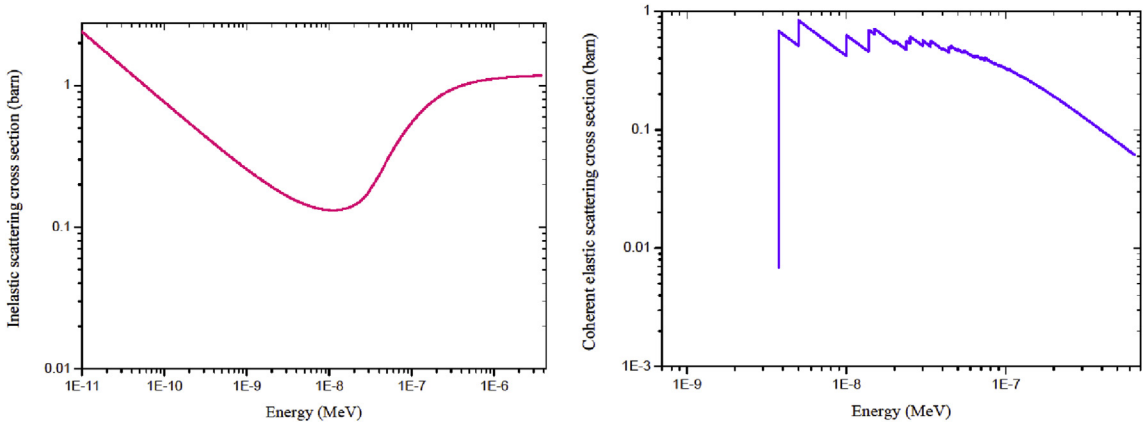

Fig. 4. Inelastic scattering cross section and coherent elastic scattering cross section of LiF at 350 K.

value and shows some 1/E drops off (see the right of Figs. 3 and 4), this trend is consistent with the results of other researchers (Hawari and Gillete, 2014; MacFarlane, 1994).

When the temperature of 2LiF-BeF_2 is above 774 K, the thermal-neutron scattering for liquid fluoride salt can be represented by combining a solid-type spectrum of rotational and vibrational modes $S_s(\alpha,\beta)$ with a diffusion term $S_t(\alpha,\beta)$:

$$S(\alpha,\beta) = S_t(\alpha,\beta)e^{-\alpha\lambda_s} + \int_{-\infty}^{\infty} S_t(\alpha,\beta\prime)Ss(\alpha,\beta-\beta\prime)\mathrm{d}\beta\prime \tag{15}$$

Based on the effective width model for the diffusion term: (Egelstaff and Schofield, 1962)

$$S_t(\alpha,\beta) = \frac{2c\omega_t\alpha}{\pi}\exp\left[2c^2\omega_t\alpha - \beta/2\right]\frac{\sqrt{c^2+0.25}}{\sqrt{\beta^2+4c^2\omega_t^2\alpha^2}}K_1\left(\sqrt{c^2+0.25}\sqrt{\beta^2+4c^2\omega_t^2\alpha^2}\right) \tag{16}$$

where $K_1(x)$ is a modified Bessel function of the second kind, and both the translational weightω_t and the diffusion constant c are input data for LEAPER code, a module of the Nuclear data processing code NJOY (MacFarlane and Muir, 1994). Diffusion constants c of F, Li and Be are calculated by molecular dynamics simulation code DL_POLY based on transferable rigid-ion model (TRIM). (Smith et al., 2002). The PACKMOL software is used for DL_POLY to obtain the initial configuration of each composition by placing the appropriate number of atoms randomly without any overlap. The diffusion coefficient F, Li and Be are shown in Fig. 5. Subsequently, the thermal-neutron inelastic scattering cross sections of F, Li and Be in 2LiF-BeF_2 are generated by NJOY to supply ACE format continuous energy cross-section library for Serpent and WIMS

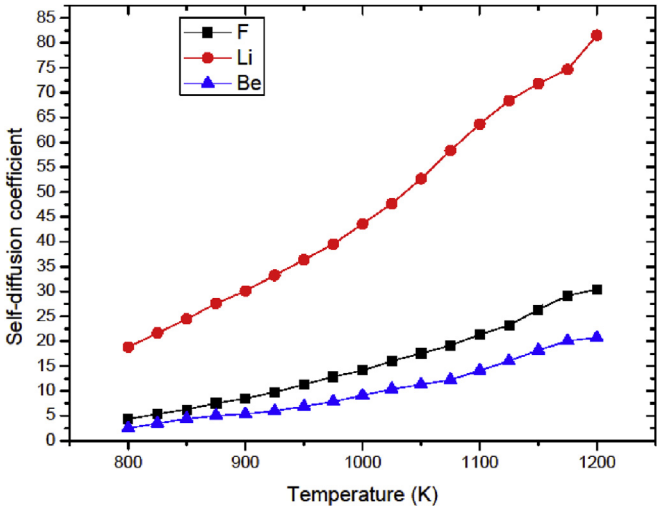

Fig. 5. Self-diffusion coefficient as a function of temperature.

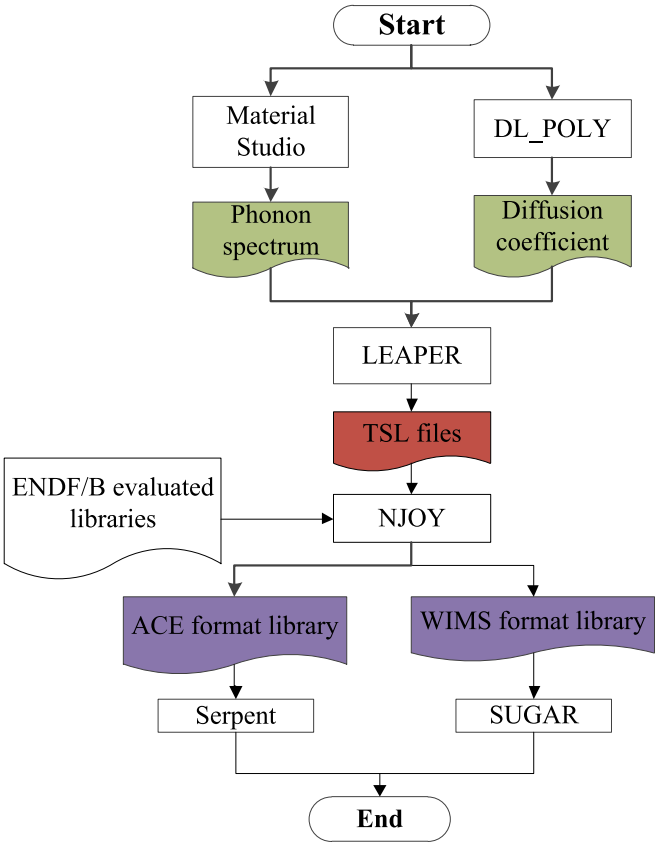

Fig. 6. Scheme of evaluating TSL files and processing ACE and WIMS format libraries of liquid 2LiF-BeF_2.

format multi-group cross-section library for SUGAR, as shown in Fig. 6.

Fig. 7 shows the continues energy thermal-neutron scattering cross sections of F, Li and Be in 2LiF-BeF_2, which will be used in the following sections. It is found that the thermal-neutron scattering cross sections of F, Li and Be in 2LiF-BeF_2 are larger than those of F, Li and Be free atom. In the previous studies on PB-FHR (Qin et al., 2016), only the scattering cross sections of F, Li and Be free atom were used in the critical calculation which would lead to an overestimation of the criticality calculation results. The thermal-neutron scattering effect of the 2LiF-BeF_2 in the PB-FHR would be quantified by comparing the critical calculation result with and without the thermal scattering cross-section libraries of 2LiF-BeF_2.

Before performing the Monte-Carlo calculations, the accuracy of the thermal scattering cross sections of F, Li and Be in 2LiF-BeF_2 were verified. The inelastic scattering cross section of 2LiF-BeF_2 at 774 K generated by this work were compared with that of the reference (Mei et al., 2013) in Fig. 8, which indicates a good agreement between them. This illustrates the thermal-neutron scattering cross sections of F, Li and Be in 2LiF-BeF_2 were correctly processed. Then the k_{inf} is calculated by Serpent with the explicit random model and thermal-neutron scattering cross sections of in 2LiF-BeF_2, it is listed in Table 4 and denoted by 'Ref. + TSL'. Compared with the 'Reference' scheme (using the explicit random model and without the thermal-neutron scattering cross sections of F, Li and Be), the 'Ref. + TSL' scheme result in a decrease of k_{inf} ranging from 104 to 383 pcm for different TPF and temperature. The main reason of the phenomenon is that the thermal-neutron scattering effect of 2LiF-BeF_2 makes spectrum harder at thermal energy range (see Fig. 9), which leads to a decrease of the neutron fission rate of ^{235}U at thermal energy range.

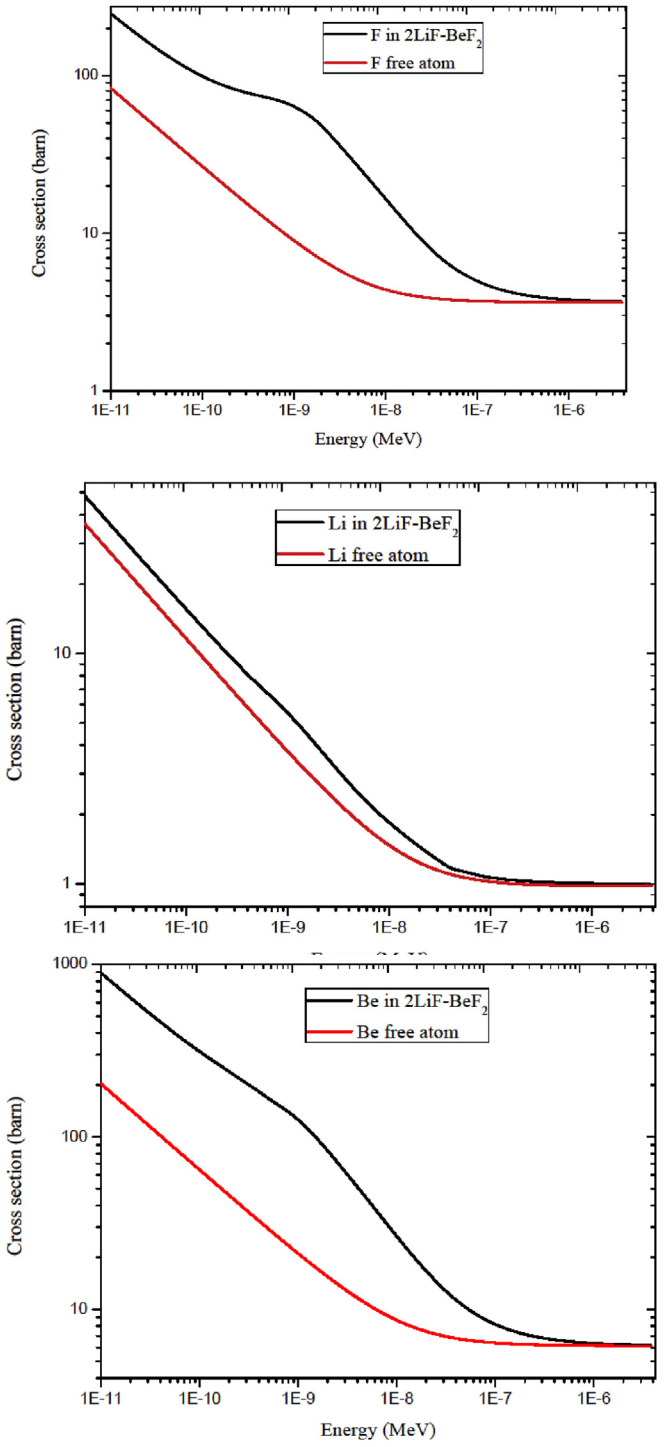

Fig. 7. Inelastic scattering cross sections of F, Li and Be in 2LiF-BeF_2 compared with that of F, Li and Be free atom at 900 K.

4. Resonance elastic scattering effect

Recent studies show that ignoring the resonance elastic scattering effect may result in a significant underestimation of resonance absorption of the heavy nuclei and overestimation of k_{inf}. The Doppler Broadening Rejection Correction (DBRC) method has been

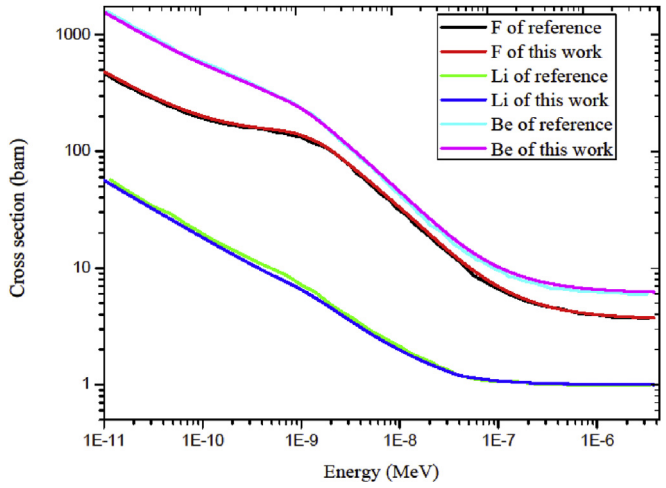

Fig. 8. Verification of inelastic scattering cross sections of F, Li and Be at 774 K.

Table 4
Influence of thermal-neutron scattering on k_{inf} for different TPF and coolant temperatures.

TPF/Pebble	5.02%	7.00%	10.0%	15.0%	30.0%
Temperature (coolant: 300 K, other material: 1000 K)					
Reference	1.48251	1.48937	1.46288	1.40067	1.25404
Ref. +TSL	1.48083	1.48618	1.45912	1.39596	1.24924
Difference (pcm)	−113	−214	−257	−336	−383
Temperature (coolant: 600 K, other material: 1000 K)					
Reference	1.48234	1.48885	1.46211	1.39956	1.25372
Ref. +TSL	1.48078	1.48616	1.45882	1.39539	1.24946
Difference (pcm)	−105	−181	−225	−298	−340
Temperature (coolant: 900 K, other material: 1000 K)					
Reference	1.48245	1.48827	1.46136	1.39876	1.25290
Ref. +TSL	1.48091	1.48596	1.45883	1.39559	1.24927
Difference (pcm)	−104	−155	−173	−227	−290

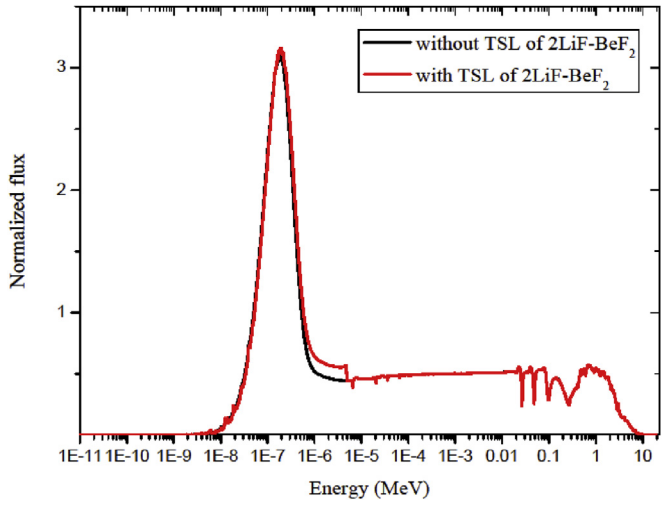

Fig. 9. Comparison of the normalized flux between the explicit random model without and with thermal-neutron scattering data library of F, Li and Be in 2LiF-BeF_2.

implemented in Serpent to quantify the resonance elastic scattering effect. The DBRC sampling algorithm of the target velocity is based on (Becker et al., 2009b):

$$P(V,\mu) = C\left\{\frac{\sigma_s(v_r,0)}{\sigma_s^{\max}\left(v_\xi,0\right)}\right\} \times \left\{\frac{v_r}{v+V}\right\} \times \left\{\frac{\left(2\beta^4\right)V^3 e^{-\beta^2V^2} + \left(\beta v\sqrt{\pi}/2\right)\left(4\beta^3/\sqrt{\pi}\right)V^2 e^{-\beta^2V^2}}{1+\beta v\sqrt{\pi}/2}\right\} \quad (17)$$

where

$$C = \frac{\sigma_s^{\max}\left(v_\xi,0\right)\left(1+\beta v\sqrt{\pi}/2\right)}{\sigma_s(v,T)\beta v\sqrt{\pi}} \quad (18)$$

C is the normalization constant, V is the speed of the target nucleus, μ is the cosine of the angle between the velocities vectors of the target nucleus and neutron, $\sigma MAX\ S(v_\xi,0)$ is the maximum value of elastic scattering cross sections within a range of the dimensionless speed, v_r is the relative speed between incident neutron and target nucleus, v is the neutron speed. The last factor of Eq. (17) is the weighted sum of two probability density functions from which the velocity of the target is sampled. The $v_r/(v+V)$ and $\sigma_S(v_r,0)/\sigma MAX\ S(v_\xi,0)$ are the two rejection tests applied to the sampled velocity of the target. The normalized scattering kernels of ^{238}U with and without the DBRC method are compared in Fig. 10. It is found that neutron up-scattering is enhanced in the low energy wing of the first resonance peak at 6.76 eV and ignoring the resonance elastic scattering effect results in a significant underestimation of the resonance absorption of the ^{238}U.

Then the k_{inf} was calculated by Serpent with the DBRC method as listed in Table 5 and denoted by 'Ref. + DBRC' scheme. Compared with the 'Reference' scheme, using the 'Reference + DBRC' scheme result in a decrease of k_{inf} ranging from 107 to 437 pcm for fuel temperature at 1000 K and 134–622 pcm for fuel temperature at 1200 K, the difference introduced by the resonance elastic scattering effect ascends with the increasing TPF and temperature It can be explained by the fact that ignoring the resonance elastic scattering effect results in a significant underestimation of the resonance absorption of the ^{238}U.

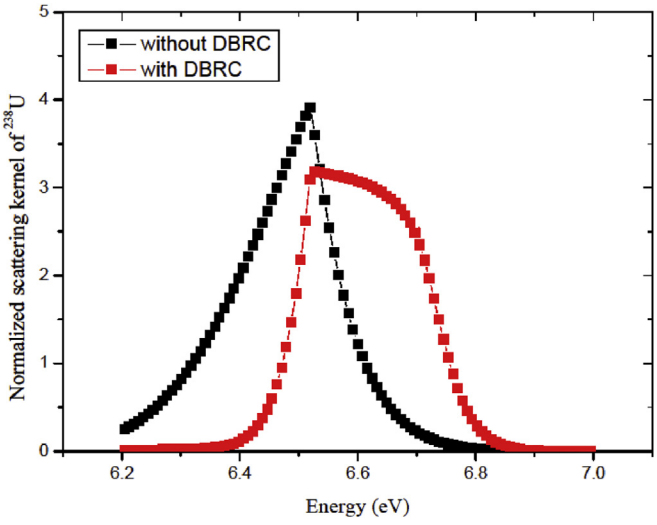

Fig. 10. Normalized scattering kernel of ^{238}U with incident energy at 6.52 eV.

Table 5
Influence of resonance elastic scattering on k_{inf} for different TPF and fuel temperatures.

TPF/Pebble	5.02%	7.00%	10.0%	15.0%	30.0%
Temperature (coolant: 900 K, other material: 1000 K)					
Reference	1.48245	1.48827	1.46136	1.39876	1.25290
Ref. +DBRC	1.48086	1.48614	1.45842	1.39474	1.24743
Difference (pcm)	−107	−143	−201	−287	−437
Temperature (coolant: 900 K, other material: 1200 K)					
Reference	1.47224	1.47617	1.44770	1.38287	1.23567
Ref. +DBRC	1.47027	1.47340	1.44368	1.37783	1.22798
Difference (pcm)	−134	−188	−278	−364	−622

5. The total impact of the thermal-neutron scattering effect and resonance elastic scattering effect

Finally, the k_{inf} was calculated by Serpent with the explicit random model, thermal-neutron scattering data of 2LiF-BeF_2 and the DBRC method when coolant temperature at 900 K and other materials temperature at 1000 K. The results are listed in Table 6 and denoted by 'Ref. + TSL + DBRC' scheme. By taking into account the two effects together, the k_{inf} of FHR pebble unit cells decrease by 204–747 pcm. It is found that the difference introduced by the thermal-neutron scattering effect of 2LiF-BeF_2 and the resonance elastic scattering effect together is approximately addible of the differences caused by the individual effect, as shown in Fig. 11. When all the effects are considered, the final k_{inf} denoted by 'Ref. + TSL + DBRC' is the most accurate. It is found that the thermal-neutron scattering effect and the resonance elastic scattering effect manifest negative effects. Moreover the absolute value of k_{inf} differences caused by the thermal scattering effect of 2LiF-BeF_2 and the resonance elastic scattering effect of heavy nuclide increase with the increasing TPF. It can be explained that both of the fission rate differences of ^{235}U and the capture rate difference of ^{238}U increase with the increase in TPF, as shown in Figs. 12 and 13. Because the thermal-neutron scattering effect impacts the thermal energy range while the resonance elastic scattering effect affects the epithermal energy range, the impacts of the two negative effects would not interfere with each other.

In order to show the fact that the thermal-neutron scattering effect and resonance elastic scattering effect would not cancel each other by using both the Monte Carlo method and deterministic method together, the impact k_{inf} of the PB-FHR pebble unit cell was also calculated by SUGAR to quantify thermal-neutron scattering effect of 2LiF-BeF_2 and the resonance elastic scattering effect of heavy nuclide. SUGAR has been developed by the Nuclear Engineering Computational Physics Laboratory at Xi'an Jiaotong University to perform the deterministic one dimensional or two dimensional arbitrary geometry sub-group resonance and neutron transport calculation (Cao et al., 2011; He et al., 2016). To consider the thermal-neutron scattering effect of 2LiF-BeF_2, the WIMS

Table 6
Impact of the thermal-neutron scattering effect and resonance elastic scattering effect on k_{inf}.

TPF/Pebble	k_{inf} (difference)				
	5.02%	7.00%	10.0%	15.0%	30.0%
Reference	1.48245	1.48827	1.46136	1.39876	1.25290
Ref.+TSL	1.48091	1.48596	1.45883	1.39559	1.24927
(Difference, pcm)	(−104)	(−155)	(−173)	(−227)	(−290)
Ref.+DBRC	1.48086	1.48614	1.45842	1.39474	1.24743
(Difference, pcm)	(−107)	(−143)	(−201)	(−287)	(−437)
Ref.+TSL + DBRC	1.47942	1.48414	1.45593	1.39158	1.24356
(Difference, pcm)	(−204)	(−278)	(−372)	(−513)	(−747)

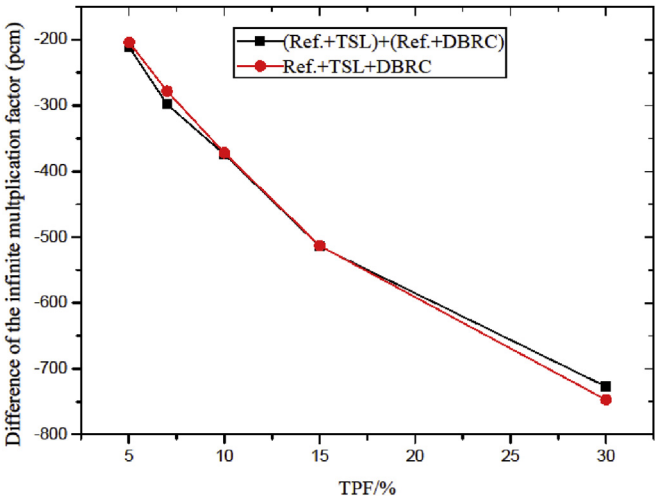

Fig. 11. The sum of the impact of thermal scattering effect of 2LiF-BeF_2 and resonance elastic scattering effect of heavy nuclide respectively, and the impact of considering the two effects simultaneously.

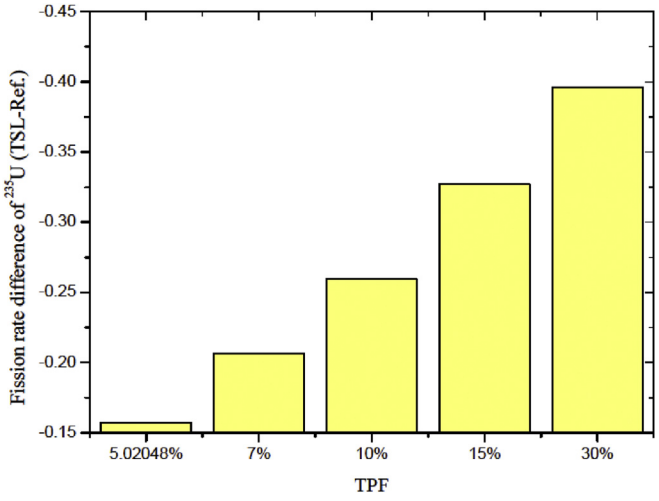

Fig. 12. The total fission reaction rate difference of the ^{235}U by 'TSL − Reference' for different TPF.

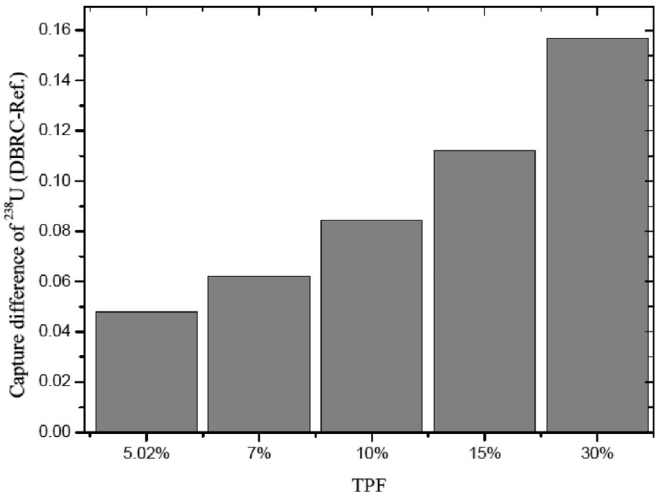

Fig. 13. The total capture reaction rate difference of the ^{238}U by 'DBRC − Reference' for different TPF.

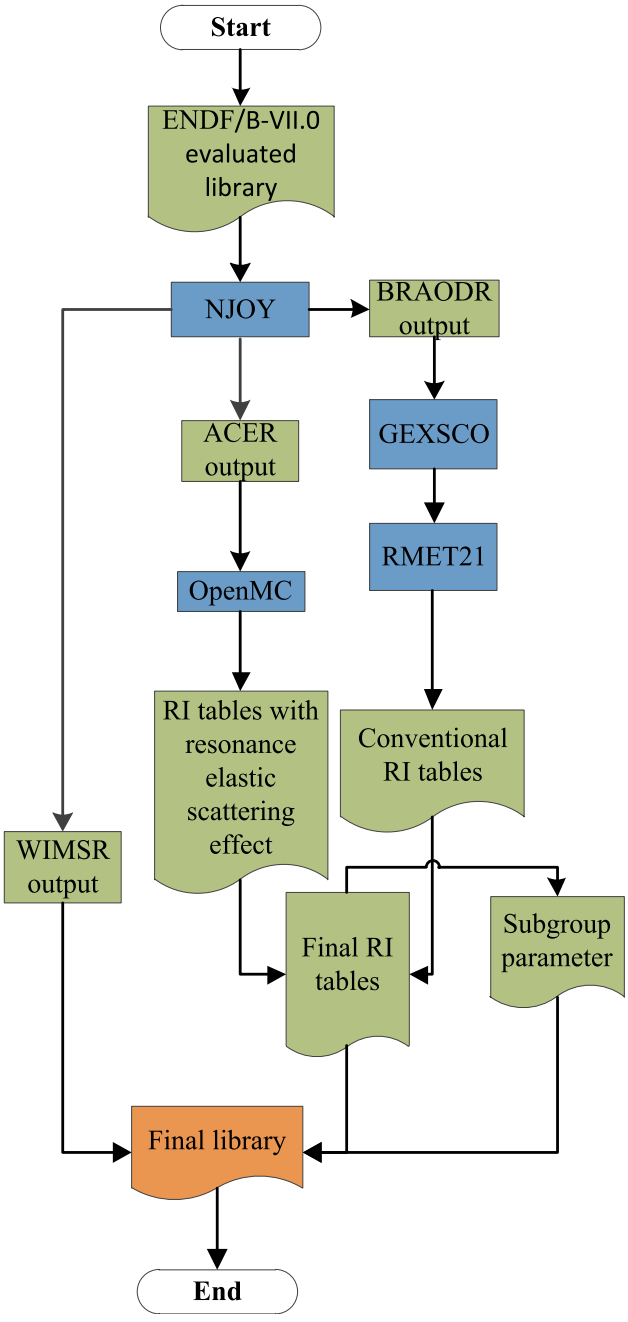

Fig. 14. Scheme of processing the sub-group library for the deterministic calculation code SUGAR. The Resonance Integral tables and probability tables with or without resonance elastic scattering effect of ^{238}U are generated by the Monte-Carlo transport code OpenMC (Romano and Forget, 2013), the Resonance Integral (RI) tables and probability tables without resonance elastic scattering effect of the other nuclei are generated by the resonance parameters calculation code GEXSCO and RMET21 (Francisco, 2001).

format multi-group thermal-neutron scattering library of 2LiF-BeF_2 for SUGAR has been generated as shown in Fig. 6. On account of the double heterogeneous of a pebble-bed fuel unit cell, SUGAR was updated to deal with the pebble-bed unit cell geometry and the DBRC method has been implemented in SUGAR to consider the resonance elastic scattering effect, the resonance elastic scattering correction factor can be obtained by Eq. (19):

$$f_{g,k}(\sigma_b, T) = \frac{\sigma_{g,k}^{DBRC}(\sigma_B, T)}{\sigma_{g,k}^{free}(\sigma_B, T)} \tag{19}$$

where the self-shielded cross sections with and without the resonance elastic scattering effect are obtained by the OpenMC code. Before performing the deterministic calculation by SUGAR, the sub-group dada library for SUGAR should be processed. The scheme of generating the sub-group dada library for SUGAR is summarized in Fig. 14.

The comparison results are listed in Table 7, which indicates that both Serpent and SUGAR can accurately deal with the thermal-neutron scattering effect of 2LiF-BeF_2 and the resonance elastic scattering effect of heavy nuclide for the PB-FHR pebble unit cell. In other words, both the Monte Carlo method and deterministic method are used to show the fact that the thermal-neutron scattering effect and resonance elastic scattering effect is addible.

6. Conclusion

In this work, the stochastic effect is analyzed by applying the explicit random modeling approach and CLS method. An in-house packing code PACK is developed to cooperate with Serpent to perform the Monte-Carlo simulation of PB-FHR pebble unit cell with randomly distributed TRISO coated-fuel particles. The thermal-neutron scattering effect of 2LiF-BeF_2 is taken into account by a new thermal-neutron scattering data library of 2LiF-BeF_2. The thermal-neutron scattering library is evaluated and processed by the frequency spectrum calculation code CASTEP, the molecular dynamics simulation code DL_POLY and the nuclear data processing code NJOY. The resonance elastic scattering effect is considered by using the Doppler Broadening Rejection Correction (DBRC) method.

For the PB-FHR pebble unit cells with different TRISO packing factor (TPF), the explicit random modeling approach can accurately deal with the stochastic geometry, the original CLS model implemented in Serpent seems to work best for low packing fractions. After using the correction technique, the difference between explicit random method and CLS method decrease significantly for high packing fraction. For the explicit random modeling PB-FHR pebble unit cells with randomly distributed TRISO coated-fuel particles, the thermal-neutron scattering effect of 2LiF-BeF_2 makes spectrum becoming harder at thermal energy range and leads to a growing decrease of the neutron fission reaction rate of ^{235}U with the increase in TPF which leads to a growing decreasement of the k_{inf} ranging from 104 to 290 pcm with the increasing

Table 7
Impact of the thermal-neutron scattering effect and resonance elastic scattering effect on k_{inf} by using Serpent and SUGAR.

Codes	Serpent	SUGAR	Relative bias (%)
Reference	1.48245	1.485105	0.18
Ref.+TSL (Difference, pcm)	1.48091(−104)	1.483561(−104)	0.19
Ref.+DBRC (Difference, pcm)	1.48086(−107)	1.483372(−117)	0.17
Ref.+TSL + DBRC (Difference, pcm)	1.47942(−204)	1.481512(−242)	0.14

TPF. The resonance elastic scattering effect results in a growing increasement of the resonance absorption of the ^{238}U with the increasing TPF which leads to a growing decreasement of the k_{inf} ranging from 107 to 437 pcm with the increasing TPF. In addition, the thermal-neutron scattering effect works in the thermal energy range while the resonance elastic scattering effect works in the epithermal energy range. Hence these two effects would not interfere with each other and the total impact of the two effects is addible, the sum of the thermal-neutron scattering effect and resonance elastic scattering effect result in a decreasement of k_{inf} ranging from 204 to 747 pcm.

The stochastic characteristics of the randomly distributed TRISO coated-fuel particles, the thermal-neutron scattering effect of the fluoride-salt and the resonance elastic scattering effect of ^{238}U are important physical effects in PB-FHR. It is necessary to take into account these three effects carefully in the engineering design of the PB-FHR core and the total impact of the three effects on full-scale reactor core parameters needs to be further analyzed.

Acknowledgement

The authors wish to thank the National Natural Science Foundation of China (Grant No. 11522544) for financial support.

References

Becker, B., Dagan, R., Broeders, C.H.M., 2009a. Improvement of the resonance scattering treatment in MCNP in view of HTR calculations. Ann. Nucl. Energy 36, 281–285.
Becker, B., Dagan, R., Lohnert, G., 2009b. Proof and implementation of the stochastic formula for ideal gas, energy dependent scattering kernel. Ann. Nucl. Energy 36, 470–474.
Cao, L., Wu, H., Liu, Q., Chen, Q., 2011. Arbitrary Geometry Resonance Calculation Using Subgroup Method and Method of Characteristics, in: M&C 2011. Rio de Janeiro, RJ, Brazil (on CD-ROM).
Egelstaff, P.A., Schofield, P., 1962. On the evaluation of the thermal-neutron scatting law. Nucl. Sci. Eng. 12, 260–270.
Francisco, L., 2001. NRSC: Neutron Resonance Spectrum Calculation System, Version 2001.0 (Centro Atómico Bariloche, CNEA, ARGENTINA).
Fratoni, M., 2008. Development and Applications of Methodologies for the Neutronic Design of the Pebble Bed Advanced High Temperature Reactor (PB-AHTR). University of California, Berkeley. Ph.D. thesis.
Greene, S.R., Gehin, J.C., Holcomb, D.E., et al., 2010. Pre-conceptual Design of a Fluoride-salt-cooled Small Modular Advanced High-temperature Reactor (SmAHTR). Oak Ridge National Laboratory. ORNL/TM-2010/199.
Griesheimer, D.P., 2010. Analysis of distances between inclusions in finite binary stochastic materials. J. Quant. Spectrosc. Radiat. Transf. 577–598.
Hawari, A.I., Gillete, V.H., 2014. Inelastic thermal neutron scattering cross sections for reactor-grade graphite. Nucl. Data Sheet 118, 178.
He, Q., Cao, L., Wu, H., Zu, T., 2016. Improved resonance calculation of fluoride salt-cooled high-temperature reactor based on subgroup method. Ann. Nucl. Energy 13 (2), 132–140.
Holcomb, D.E., Ilas, D., Varma, V.K., Cisneros, A.T., Kelly, R.P., Gehin, J.C., 2011. Core and Refueling Design Studies for the Advanced High Temperature Reactor. Oak Ridge National Laboratory. ORNL/TM-2011/365.
IAEA, 2003. Evaluation of High Temperature Gas Cooled Reactor Performance: Benchmark Analysis Related to Initial Testing of the HTTR and HTR-10. Nuclear Power Technology Development Section, International Atomic Energy Agency. IAEA-TECDOC-1382, 255.
Ji, W., Martin, W.R., 2008. Application of chord length sampling to VHTR unit cell analysis. In: Proceeding of International Conference on the Physics of Reactor (PHYSOR2008) (Interlaken, Switzerland).
Krumwiede, D.L., Scarlat, R.O., Choi, J.K., Phan, T.M., Peterson, P.F., 2013. Three dimensional modeling of the pebble-bed fluoride-salt-cooled, high temperature reactor (PB-FHR) commercial plant design. In: Proceedings of the American Nuclear Society 2013 Winter Meeting.
Leppänen, J., 2012. Serpent- a Continuous-energy Monte Carlo Reactor Physics Burnup Calculation Code. VTT Technical Research Centre of Finland. User's Manual 2012.
Liang, C., Ji, W., 2011. Parameter sensitivity study on the accuracy of chord length sampling method. Trans. Am. Nucl. Soc. 105, 495–497.
Liang, C., Ji, W., Brown, Forrest B., 2012. Chord length sampling method for analyzing VHTR unit cells in continuous energy simulations. In: Proceeding of International Conference on the Physics of Reactor (PHYSOR2012) (Knoxville, Tennessee, USA).
Liu, S., She, D., Liang, J., Wang, K., 2015a. Development of random geometry capability in RMC code for stochastic media analysis. Ann. Nucl. Energy 85, 903–908.
Liu, S., She, D., Liang, J., Wang, K., 2015b. Implementation of Explicit Modeling Approach in RMC Code for Stochastic Media Analysis, vol. 112. Transactions of the American Nuclear Society. San Antonio, Texas, June 7–11.
Liu, L., Zhang, D., Lu, Q., Wang, K., Qiu, S., 2016. Preliminary neutronic and thermal-hydraulic analysis of a 2 MW Thorium-based molten salt reactor with solid fuel. Prog. Nucl. Energy 86, 1–10.
MacFarlane, R.E., 1994. New Thermal Neutron Scattering Files for ENDF/B-VI Release 2, LA-12639-MS, 59.
MacFarlane, R.E., Muir, D.W., 1994. The NJOY Nuclear Data Processing System, Version 91, Los Alamos National Laboratory Report LA-12740-M.
Mei, L., Cai, X., Jiang, D., et al., 2013. The investigation of thermal-neutron scattering data for molten salt Flibe. J. Sci. Technol. 50 (7), 682–688.
Mori, T., Okumura, K., Nagaya, Y., Ando, H., 2000. Monte Carlo analysis of HTTR with the MVP statistical geometry model. Trans. Am. Nucl. Soc. 83, 283.
Murata, I., Mori, T., Nakagawa, M., 1996. Continuous energy monte carlo calculations of randomly distributed spherical fuels in high-temperature gas-cooled reactors based on a statistical geometry model. Nucl. Sci. Eng. 123, 96–109.
Murata, I., Takahashi, A., Mori, T., Nakagawa, M., 1997. New sampling method in continuous energy monte carlo calculation for pebble bed reactors. J. Nucl. Sci. Technol. 34 (8), 734–744.
Qin, W., Yang, K., Chen, J., Cai, X., 2016. Dancoff factor analysis for pebble bed fluoride salt cooled high temperature reactor. Prog. Nucl. Energy 88, 332–339.
Refson, K., 2004. CASTEP User Guide. CCLRC Rutherford Appleton Laboratory.
Reinert, D.R., 2010. Investigation of stochastic radiation transport methods in binary random heterogeneous mixtures. Nucl. Sci. Eng. 166, 167–174.
Romano, P.K., Forget, B., 2013. The OpenMC Monte Carlo particle transport code. Ann. Nucl. Energy 51, 274–281.
Scarlat, R.O., Peterson, P.F., Jun. 2013. The current status of fluoride salt cooled high temperature reactor (FHR) technology and its overlap with HIF target chamber concepts. Nucl. Instrum. Methods Phys. Res. A 733, 57–64.
She, D., Xie, F., Li, F., Liu, S., Wang, K., 2015. Explicit modeling of double-heterogeneous pebble-be reactors with the RMC code. In: Proc. M&C+SNA+MC 2015. Nashville, TN, April 19–23.
SINAP, 2012. Pre-conceptual Design of 2MW Pebble-bed Fluoride Salt Coolant High Temperature Test Reactor. Shanghai Institute of Applied Physics, Shanghai.
Smith, N., et al., 2001. The Current Status and Future Plans for the Monte Carlo Codes MONK and MCBEND. Advanced Monte Carlo for Radiation Physics, Particle Transport Simulation and Applications. Springer Berlin Heidelberg, pp. 637–642.
Smith, W., Yong, C., Rodger, P., 2002. DL_POLY: Application to molecular simulation. Mol. Simul. 28 (5), 385–471.
Varma, V.K., Holcomb, D.E., Peretz, F.J., et al., 2012. AHTR Mechanical, Structural, and Neutronic Pre-conceptual Design. ORNL, Oak Ridge, TN. ORNL/TM-2012/320.
Xiao, Y., Hu, L., Forsberg, C., Qiu, S., Su, G., Chen, K., Wang, N., 2014. Analysis of the limiting safety system settings of a fluoride-salt-cooled high-temperature test reactor. Nucl. Technol. 187, 221–234.